Audio Engineering Society

Convention Paper 8215

Presented at the 129th Convention
2010 November 4–7 San Francisco, CA, USA

Dynamic Motion of the Corrugated Ribbon in a Ribbon Microphone

Daniel Moses Schlessinger[1], Jonathan S. Abel[2]

[1] *Sennheiser DSP Research Laboratory, Palo Alto, CA, 94306 USA*

[2] *CCRMA, Department of Music, Stanford University, Stanford, CA, 94305 USA*

Correspondence should be addressed to Daniel Schlessinger (daniel.schlessinger@sennheiser.com)

ABSTRACT

Ribbon microphones are known for their warm sonics, owing in part to the unique ribbon motion induced by the sound field. Here the motion of the corrugated ribbon element in a sound field is considered, and a physical model of the ribbon motion is presented. The model separately computes propagating torsional disturbances and coupled transverse and longitudinal disturbances. Each propagation mode is implemented as a mass-spring model where a mass is identified with a ribbon corrugation fold. The model is parameterized using ribbon material and geometric properties. Laser vibrometer measurements are presented, revealing stiffness in the transverse and longitudinal propagation, and showing close agreement between measured and modeled ribbon motion.

1. INTRODUCTION

Ribbon microphones were among the first microphones developed [1], and are still sought after today. The unique sonics of ribbon microphones gave us classic vocal recordings from the 1950's, and many still consider them to be an indispensable part of any full microphone locker [2]. Ribbon mics are often described as having a "warmth" or "smoothness," which likely results from a combination of the frequency response and transducer nonlinearities.

Designed by Harry Olson for RCA in the 1930s, early ribbon microphones such as the RCA 77 series (Fig. 1) featured an aluminum ribbon having an elongated rectangular design incorporating folds or corrugations oriented perpendicular to the ribbon axis [3]. This corrugated ribbon design can also be found in the classic Coles 4038 and the RCA44A.

The mechanism of the ribbon microphone is straightforward: a thin metal filament is set in motion by incident sound waves, and the velocity of the ribbon

Fig. 1: Classic RCA 77D Microphone (left) [21], and corrugated ribbon from a Nady RSM-4 ribbon microphone (right). The corrugations stiffen the ribbon against off-axis motion.

in a permanent magnetic field creates a voltage signal [3]. The corrugations stiffen the ribbon against off-axis motion and keep the ribbon flexible throughout its length [1]. In order to better understand the sound of the classic ribbon mics, in this paper we explore the motion of the corrugated ribbon in response to a sound field, and present a physical model of the ribbon motion.

Traditional analysis of the ribbon microphone [3][4][5][6] assumes the ribbon to behave as a single lumped mass connected to a spring, oscillating at a single resonant frequency, typically in the range of 15–40Hz [7]. This analysis is adequate for explaining the general response of the ribbon microphone, which Olson describes as having a "uniform response frequency characteristic over the entire audio frequency range, and a uniform directivity pattern over the entire audio frequency range" [3]. Ribbon motion is driven by the difference in pressure between front and back of the ribbon, which, in turn, results from a short acoustic delay D between the incident sound waves at the front and back of the ribbon, as seen in Fig. 2. The differential pressure ΔP, as a function of wavenumber k and angle of sound incidence θ and normalized by the on-axis ΔP_{max} is accordingly

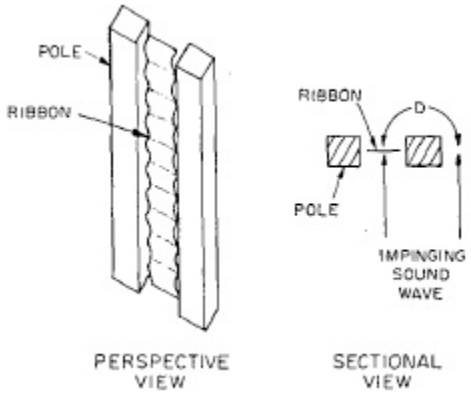

Fig. 2: Diagram of ribbon, magnets ('poles') and impinging sound wave (taken from [3], page 264). The geometry causes a small time delay D between sound waves arriving at the front and the back of the ribbon.

$$\Delta P = \frac{\sin[(kD/2)\cos\theta]}{kD/2}. \qquad (1)$$

Note that for small values of kD the $\cos\theta$ term above produces the well known figure of eight polar pattern seen in Fig. 3.

The lumped mass model also predicts the flat frequency response. From on-axis source P, differential pressure ΔP at frequency ω and speed of sound c is described by the equation

$$\Delta P = 2P\cos(\omega t)\sin\left[\frac{\omega D}{2c}\right], \qquad (2)$$

where the substitution $k = \omega/c$ has been made, cf. ([3], equation 1). ΔP maintains a 6dB per octave highpass characteristic at low frequencies (Fig. 4). The output signal is proportional to the ribbon velocity $\dot{x}$, which for a ribbon with surface area A and mass m_R (which Olson lumps with the mass of air m_A, on either side), can be described in the lumped mass approach by

$$\dot{x} = \frac{\Delta P A}{j\omega(m_R + m_A)}, \qquad (3)$$

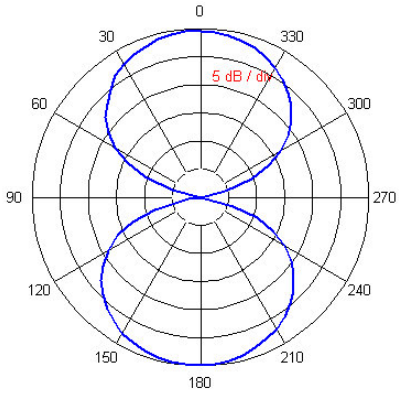

Fig. 3: Characteristic figure-of-eight pattern of Coles 4038 ribbon microphone measured at 1kHz. Nulls are especially strong in ribbon microphones for off-axis sound sources, as such sources produce little differential pressure

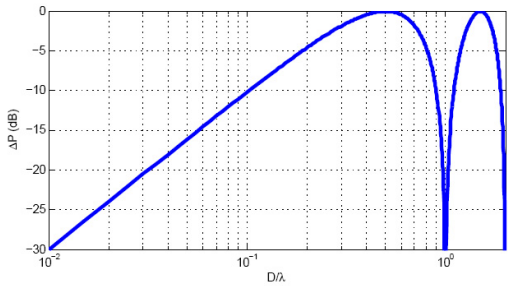

Fig. 4: Differential sound field pressure driving force ΔP as a function of acoustic path length D and wavelength λ. The time delay D shown in Fig. 2 creates a 6dB per octave highpass for low and mid frequencies, and produces a spectral null as the wavelength λ approaches D.

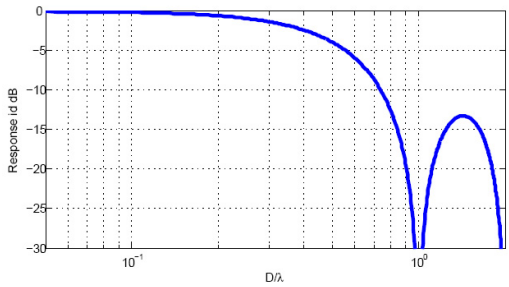

Fig. 5: Ribbon velocity of ribbon as a function of driving frequency. The 6 dB per octave highpass driving force for low frequencies shown in Fig. 4 is balanced by the 6 dB per octave lowpass due to the ribbon mass to produce a characteristic ribbon mic response. The output signal is proportional to the ribbon velocity.

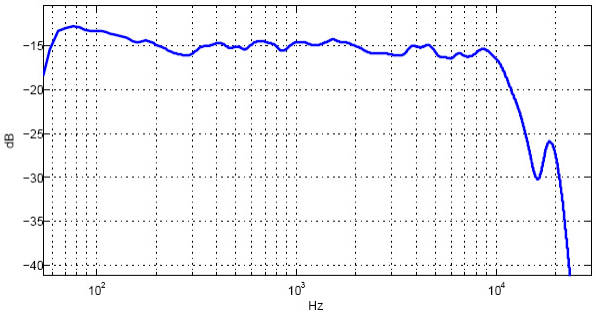

Fig. 6: Measured frequency response of a Coles 4038 ribbon microphone. Note the null and peak at frequencies above 10kHz as anticipated by Olson's lumped mass model [3] in Fig. 5.

which creates a 6dB per octave lowpass characteristic. When combined with the driving pressure highpass (Fig. 4), the velocity takes on the frequency response curve shown in Fig. 5, which shows the same general shape as the measured response of a Coles 4038 ribbon microphone shown in Fig. 6.

While the traditional lumped-mass model describes the overall frequency response of the ribbon microphone, it misses some of the nuances caused by more complex motions. Shorter and Harwood, for example, noted that in the absence of a damping screen, the ribbon microphone displays sharp resonant peaks at various harmonics of the fundamental resonance [7].

Physical models of microphones have been developed in the past. Olson created models of many types of microphones, using analog circuit equivalents of many of the acoustic and mechanical components of microphones [4]. Leach[12] and Wells[13] use SPICE to implement circuit equivalents of microphones. Roger Grinnip has recently created a thorough finite-element model of a condenser microphone, including in-depth behavior of the membrane, very accurately describes the microphone frequency response [8].

Bank and Hawksford [9][10], also employing finite element methods, presented a model of a ribbon loudspeaker which was able to show harmonic resonant characteristics of the ribbon motor.

Julian David [11] has recently built upon the work of Richard Werner [5], describing the way that the transformer and preamplifier actually alters the mechanical behavior of the ribbon in a ribbon microphone, although still a lumped mass is used to describe the basic mechanics of the ribbon.

In this paper we examine the ribbon motion in a more nuanced way. In Section 2, we consider the motion of each fold of the corrugated ribbon, and the various degrees of freedom available to it. In Section 3, we present a physical model to describe the shape of the ribbon as it evolves over time. In Section 4, we verify the results of the model through laser vibrometer measurements, and make adjustments to the model to account for behavior found in the measurements, specifically by incorporating a stiffness term.

2. RIBBON MOTION

2.1. Ribbon Vibrational Modes

Consider the motion of the corrugated aluminum ribbon suspended between two rigid terminations. Each corrugation consists of two flat ribbon sections connected by folds on either side. Five individual vibrational modes become evident (Fig. 7): transverse, side-side, longitudinal, torsional, and skew.

2.2. Modes of Vibration Considered

In order to simplify our analysis, we restrict consideration of the vibrational modes to those that contribute to the output signal, or are coupled to ones that do. This immediately allows us to reject side-side modes from consideration, because the motion is parallel to the magnetic field lines and thus do not generate voltage according to Faraday's Law. We can also eliminate the skew modes from consideration, since the motion of the ribbon folds is entirely vertical and thus any voltage induced would be perpendicular to the terminals, creating zero output signal. Torsional modes and transverse modes both fit the criteria outlined above. It is interesting to note that, in the presence of perfectly uniform magnetic field lines, symmetric torsional modes will induce no net voltage since equal parts of the ribbon are moving in opposite directions with respect to the field lines. However, since we do not assume a uniform field, these will still be considered.

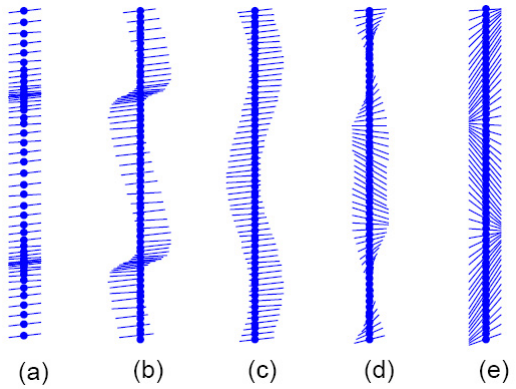

Fig. 7: Ribbon vibrational modes include (a) longitudinal, in which folds move along the ribbon axis, (b) transverse, in which the folds move perpendicular to the plane of the ribbon, (c) side-side, in which the folds move parallel to themselves in the plane of the ribbon, (d) torsional, where the folds rotate about the ribbon axis, and (e) skew, where the folds rotate about an axis that is perpendicular to the plane of the ribbon.

Longitudinal modes do not directly create a voltage across the terminals. However, as we will show later, longitudinal modes are coupled to the transverse modes, and are therefore still considered.

Thus, we restrict analysis to three modes of motion: longitudinal, transverse, and torsional modes. Analysis of these three modes as driven by both differential pressure and gravity will be considered.

3. RIBBON DYNAMICS MODEL

There are a few well known approaches for modeling the motion of thin sheets of metal. One approach applies a finite element methods, such as Bilbao, Arcas, and Chaigne used to model plate reverb [14][15]. In their work, a discrete point of excitation was used and the vibrations over time calculated at any point on the membrane. This would also be similar to the ribbon loudspeaker work by Bank and Hawksford[9], where the ribbon was modeled using a matrix of tiny mass-spring sheets, with the partial differential equations discretized. However, we would have to add spatial variations to account for the increased horizontal stiffness, nonuniform vertical propagation speed (due to contoured corrugations), and set the side and top boundaries according to stiff and open terminations.

The approach that we have chosen offers an intuitive interpretation of the pertinent parameters such as the catenary ribbon shape due to gravity and the nominal corrugation distance. We separately consider the torsional mode and the coupled transverse and longitudinal modes, and present a mass-spring model for each. In this way we hope to gain physical insight into the motion and output of the ribbon as it changes over time in a magnetic field.

3.1. Torsional Modes

Consider the way a single ribbon fold twists about the ribbon axis. We model the torsional dynamics as a series of rigid masses — one for each fold — with moments of inertia m_θ, coupled by linear torsional springs each with spring constant k_θ (see Fig. 8).

Using Newton's equation for torsional motion we can relate θ_i, the displacement of the ith fold, to the net torque applied to it from external and internal forces, τ_i, as

$$\tau_i = m_\theta \ddot{\theta}_i. \tag{4}$$

The net torque, τ_i applied to a the ith fold consists of the difference in acoustic pressure differential $\tau_{\Delta P,i}$ between the left and right halves, the damping torque, $\tau_{d,i}$, which will always oppose torsional velocity, $\dot{\theta}_i$, and the torque from the springs, τ_s.

We consider the damping torque τ_d to be caused by the viscosity of the air as well as heat generated by the twisting of the aluminum. We approximate this by implementing a damping constant, γ_θ, described as

$$\tau_d = -\gamma_\theta \dot{\theta}. \tag{5}$$

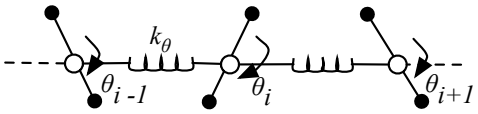

Fig. 8: Torsional mode of vibration. The ith fold with moment of inertia m_θ is rotated by the angle θ_i and coupled to adjacent folds via torsional springs with spring constant k_θ.

Using Hooke's Law to connect k_θ, the torsional spring constant, to τ_s, the torque applied to a fold from adjacent folds, we have

$$\tau_{s,i} = k_\theta[(\theta_{i+1} - \theta_i) + (\theta_{i-1} - \theta_i)], \tag{6}$$

which leads to an expression for torsional motion,

$$m_\theta \ddot{\theta} + \gamma_\theta \dot{\theta}_i - k_\theta(\theta_{i+1} - 2\theta_i + \theta_{i-1}) = \tau_{\Delta P,i} \tag{7}$$

where again $\tau_{\Delta P,i}$ is the acoustic driving torque due to the difference in pressure differential between the left and right halves of the ith fold.

This equation describes a standard "beaded string" and as the corrugation size decreases to zero it reduces to a standard string wave propagation without dispersion.

At the boundaries, we force the torsional displacements to zero, and as such any torsional waves propagating along the ribbon undergo an inverting reflection at the terminations.

3.2. Transverse/Longitudinal Modes

The transverse (along the x direction) and longitudinal (along the z direction) modes are a bit more complicated. Although the acoustic driving force in the longitudinal direction is assumed to be negligible, we assume that large displacements in the transverse direction cause the ribbon to move in the longitudinal direction, coupling the modes together. We model each ribbon section in between folds as a

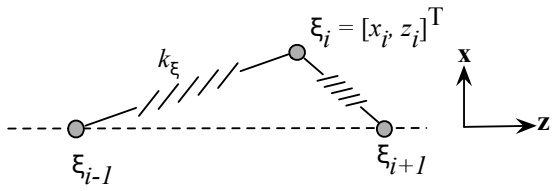

Fig. 9: Coupled transverse and longitudinal displacements. The ribbon section in between each fold is modeled as mass m_ξ with displacement vector ξ_i, which contains the longitudinal (z_i) and transverse (x_i) components, coupled by a spring with spring constant k_x.

mass m_ξ with displacement vector ξ_i, connected by a linear spring with spring constant k_ξ (Fig. 9).

The dynamics of the masses are governed by Newton's laws:

$$F_i = m_\xi \ddot{\xi}_i, \tag{8}$$

where the displacement of the ith mass has two components,

$$\xi_i = \begin{bmatrix} x_i \\ z_i \end{bmatrix}, \tag{9}$$

as does the force

$$F_i = \begin{bmatrix} F_{x,i} \\ F_{z,i} \end{bmatrix}. \tag{10}$$

The force F_i driving the motion of the ith fold is comprised of the force $F_{\Delta P,i}$ due to differential pressure on the front and back of the fold, the force $F_{s,i}$ due to the Hooke's Law, the force $F_{g,i}$ due to gravity (that at certain angles and cause the ribbon to "droop" under low tension), and the damping forces $F_{d,i}$.

For the Hooke's Law force $F_{s,i}$, we assume that the ribbon is held under extremely small but measurable tension, so there is a nonzero nominal distance L_0 between folds under zero tension which is less than the distance under normal tension.

the force on the ith mass due to Hooke's Law is

$$F_{k,i} = -k_x \left[1 - \frac{L_0}{||\xi_i - \xi_{i-1}||}\right](\xi_i - \xi_{i-1}) - k_x \left[1 - \frac{L_0}{||\xi_i - \xi_{i+1}||}\right](\xi_i - \xi_{i+1}), \tag{11}$$

where $||\xi_i - \xi_{i-1}||$ is the length between positions ξ_i and ξ_{i-1}.

The force due to gravity, $F_{g,i}$, is described by

$$F_{g,i} = m_i g \begin{bmatrix} \cos\phi \\ \sin\phi \end{bmatrix}, \tag{12}$$

where ϕ is the angle at which the ribbon is being held with respect to gravity, and g is Newton's gravitational constant.

Damping is again caused by the viscosity of the air and heat losses in the aluminum, which can be expressed in a manner similar to that of the torsional mode,

$$F_{d,i} = -\gamma_\xi \dot{\xi}_i, \tag{13}$$

where γ_ξ is the coefficient of damping.

The total equation of motion for the ith fold is

$$m_\xi \ddot{\xi}_i + \gamma_\xi \dot{\xi}_i + k_\xi(\eta_{i,i-1} + \eta_{i,i+1}) = m_i g \begin{bmatrix} \cos\phi \\ \sin\phi \end{bmatrix} + F_{\Delta P,i}, \tag{14}$$

where

$$\eta_{a,b} = \left[1 - \frac{L_0}{||\xi_a - \xi_b||}\right](\xi_a - \xi_b). \tag{15}$$

3.3. Simulated Vibrational Modes

The model enables examination of the behavior of the ribbon in a simulated sound field. All three considered modes create wave propagation along the main axis of the ribbon, generating harmonic resonances at certain frequencies. Fig. 10 shows a simulated displacement of the coupled transverse and longitudinal modes at harmonic peaks, when exposed to simulated plane waves. Excited by an on-axis plane

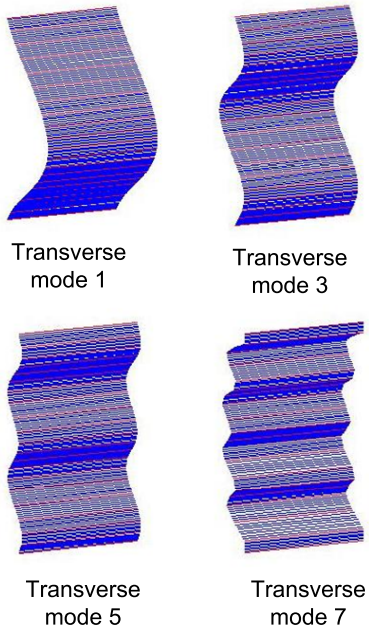

Fig. 10: Transverse modes simulated by on-axis driving pressure. Only the odd modes are stimulated by on-axis impinging sound waves.

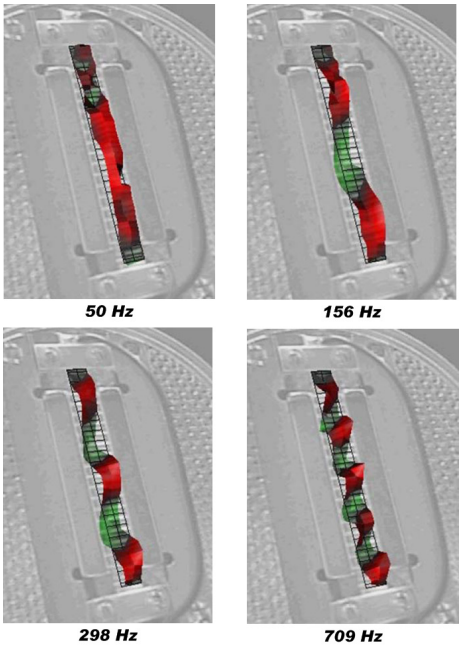

Fig. 11: Laser vibrometer snapshots of the first four odd transverse resonances are shown, corresponding to peaks in the RMS velocity spectrum in Fig. 13.

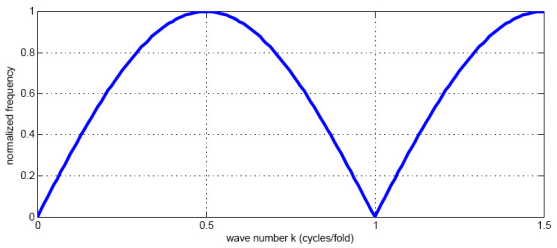

Fig. 12: Expected normalized frequency as a function of wave number k. Nulls occur where the waves propagate exactly one fold per cycle so that no net movement is detectable.

wave, the model only creates odd modes of vibration.

Furthermore, the spring-mass model predicts that the propagation velocity should slow as the propagation wavelengths approach a distance between adjacent folds. This is a type of spatial aliasing, and would take on the propagation characteristic of Fig. 12 [16]. For wavelengths shorter than the distance between folds, we would expect there to be a different propagation mode, as the aluminum itself would be bending irrespective of the fold locations.

4. LASER VIBROMETER MEASUREMENTS

Laser vibrometer measurements were carried out using a Nady RSM-4 microphone and an on-axis loudspeaker sound source. Sinusoidal sweeps were produced by the sound source while the laser vibrometer measured the velocity and displacement at three points along each corrugation.

Using the laser vibrometer data, the RMS velocity spectrum of the ribbon was computed and plotted in Fig. 13. Many resonances are visible, and snapshots of the ribbon velocity excited by the first four resonant frequencies can be seen in Fig. 11, and detail for the third resonance is seen in Fig. 14. Fig. 15 shows snapshots of the ribbon velocity excited at 298Hz as it varies over time. This behavior is very similar to that predicted by our model (Fig. 10).

There appeared to be little torsional movement present in the laser measurements, although the on-axis loudspeaker position tested was not expected to excite these nodes very significantly. The snapshots show a slight asymmetry on the left and right halves

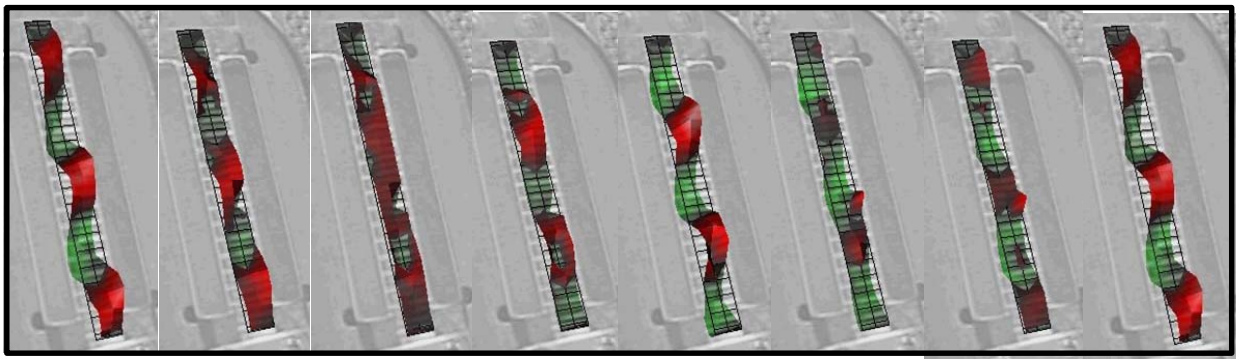

Fig. 15: Laser vibrometer images of transverse fold velocity in a 298Hz sound field is plotted over time. This corresponds to the third transverse mode of vibration. (There appears to be a "stuck pixel" on the right hand side, eighth pixel from the bottom. We believe this is due to misalignment with the laser, perhaps measuring the position of the magnet next to the desired ribbon location.)

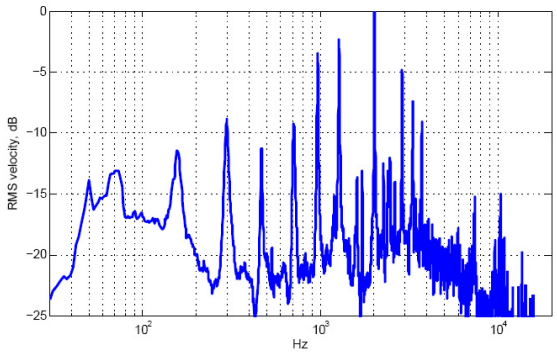

Fig. 13: Laser RMS velocity, averaged across the entire ribbon

of the ribbon velocity, but we believe this to be due to slight misalignments in the laser setup rather than the presence of significant torsional components.

4.1. Stiffness

Consider the velocity spectrum shown in Fig. 13. The peaks correspond to resonances, and these resonant frequencies below 4kHz are plotted as a function of wavenumber in Fig. 16. The slope of the frequency vs. wavenumber characteristic is the propagation speed, which appears to be increasing with wavenumber, perhaps resulting from stiffness in the ribbon.

Consider a sinusoidal disturbance $\psi(x,t)$

$$\psi(x,t) = e^{j(\omega t - kx)} \qquad (16)$$

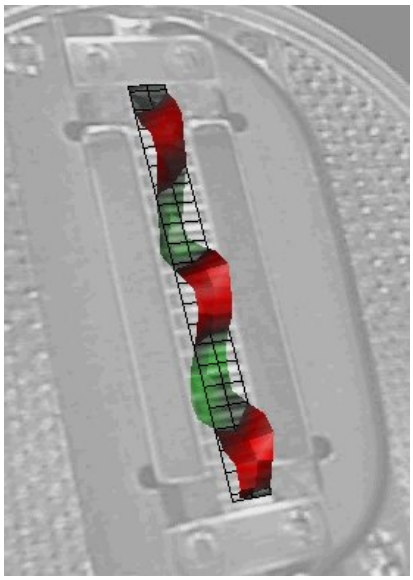

Fig. 14: Laser vibrometer snapshot of transverse fold velocity in a 298Hz sound field. This third mode of vibration corresponds to a peak seen at 298Hz in Fig. 13.

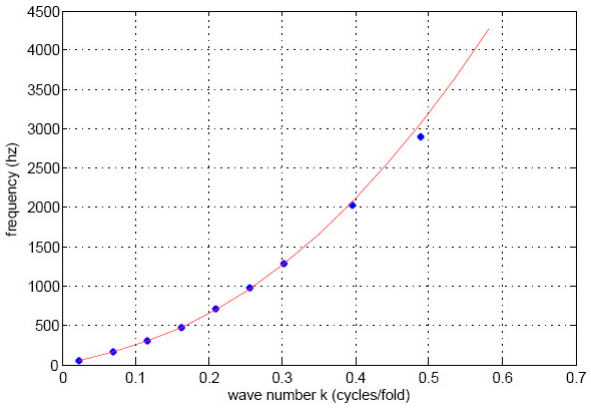

Fig. 16: Measured frequency as a function of wavenumber computed using the excited modes of vibration under 4kHz and measured ribbon dimensions to calculate wavenumber. The final points below the projected line suggests that we are beginning the downward trend predicted in Fig. 12.

propagating along a stiff string. The partial differential equation for a stiff string with damping is

$$\frac{\partial^2\psi}{\partial t^2} + \gamma\frac{\partial\psi}{\partial t} = c^2\frac{\partial^2\psi}{\partial x^2} - \beta\frac{\partial^4\psi}{\partial x^4}, \qquad (17)$$

where the constant β quantifies the stiffness. The propagation frequency ω is then a nonlinear function of the wavenumber k, described by

$$\omega^2 = c^2k^2 + \beta k^4. \qquad (18)$$

A least squares fit of the model to the data shows good agreement to a polynomial of this form, cf. Fig. 16.

The highest propagation frequencies in Fig. 16 are slightly, but measurably less than that predicted by the stiff string model, and perhaps indicate some beaded-string characteristics as in Fig. 12. This possibility may be tested with higher spatial density laser vibrometer measurements.

4.2. High Wavenumber Propagation

There appears to be another propagation region, indicated by resonances at integer multiples of 7kHz. It seems likely that these resonances are associated with high wavenumber propagation — waves traveling with wavelengths shorter than inter-fold spacing. Such a mechanism is similar to that found in a helical coil, in which a beaded string behavior is seen for wavelengths spanning many coils, and stiff string behavior is noted for higher wavelengths shorter than a coil [17].

5. SUMMARY

In this paper, we considered the dynamic motion of a corrugated ribbon in a ribbon microphone, expanding upon Olson's lumped mass analysis. We developed a physical model to better understand the motion. We verified our model using laser vibrometer measurements, and found that a stiffness term was necessary to explain the mid-frequency behavior. We also observed large wavenumber propagation, which may be modeled by a bidirectional waveguide [19].

We hope to test other microphones such as the Coles 4038 or RCA 77D, to understand if there is a qualitative difference in behavior. Furthermore, it would be interesting to study a microphone that uses a vertical corrugation pattern, such as the Beyerdynamic M260 [18]. Off-axis measurements should be taken to explore the extent to which torsional waves are excited, and all measurements should be taken at higher spatial resolutions to validate our current results.

6. ACKNOWLEDGEMENTS

We would like to thank Jim Anderson for his advice and the lending of his Coles 4038 ribbon microphone. Special thanks to Günter Rosen for sharing his considerable knowledge, and to Axel Grell and Grit Bonin for their assistance with the laser vibrometer measurements.

7. REFERENCES

[1] Harry F. Olson, "Apparatus for Converting Sound Vibrations Into Electrical Variations." U.S. Patent 1,885,001, October 1932.

[2] David Miles Huber, Robert E. Runstein *Modern Recording Techniques* Focal Press; 7 edition, October 2009.

[3] Harry Olson, "Ribbon Velocity Microphones", J. Audio Eng. Soc., vol. 18 Issue 3, pp 263-268, 1970.

[4] Harry Olson, *Applied Acoustics* 2nd Ed., Maple Press Company, York, PA, 1934.

[5] Richard E. Werner, "On Electrical Loading of Microphones", J. Audio Eng. Soc., Vol 3 Issue 4, pp 194-197, 1955.

[6] L. L. Beranek, *Acoustics* Acoustical Society of America, Woodbury, NY, 1996.

[7] D.E.L. Shorter, H. D. Harwood, *The Design of a Ribbon Type Pressure-Gradient Microphone For Broadcast Transmission*, Research Dept., BBC Engineering Division, 1955

[8] Roger S. Grinnip III, "Advanced Simulation of a Condenser Microphone Capsule", presented at the 117th AES Convention, San Francisco, CA, 2004 Oct. 28-31.

[9] G. Bank, M.O.J. Hawksford, "Advances in Computer Modeling of Ribbon Loudspeakers", presented at the 96th AES Convention, Amsterdam, The Netherlands, 1994.

[10] G. Bank, M.O.J. Hawksford, "Comparisons between the Measured and Computed Performance of Ribbon Loudspeakers", presented at the 100th AES Convention, Copenhagen, Denmark, 1996.

[11] Julian David, "Analysis of the interaction between ribbon motor, transformer, and preamplifier and its application in ribbon microphone design", presented at the 128th AES Convention, London, UK 2010 May 22-25

[12] W. Marshall Leach, Jr., "Computer-Aided Electroacoustic Design with Spice", J. Audio Eng. Soc., Vol 39, No. 7/8, 1991 July/August

[13] Collin Wells, "Modeling Electret Condenser Microphones in SPICE", http://www.engenius.net/site/zones/audiovideoZONE/technical_notes/avt_030110, accessed Aug. 25th, 2010

[14] Stefan Bilbao, "A Digital Plate Reverberation Algorithm", J. Audio Eng. Soc., Vol. 55, No. 3, March 2007.

[15] A. Bilbao, K. Arcas, and A. Chaigne,"A Physical Model for Plate Reverberation," proceedings from the IEEE Int. Conference on Acoustics, Speech and Signal Processing, vol. 5, pp. 165-168, May 2006.

[16] Thomas D. Rossing, Neville H. Fletcher, *Principles of Vibration and Sound*, 2nd Ed., Springer-Verlag, New York, 2004.

[17] L. Della Pietra and S. della Valle, *On the dynamic behaviour of axially excited helical springs,* Meccanica Volume 17, Number 1, 31-43, 1982.

[18] Michael Gayford, *Microphone Engineering Handbook*, Focal Press, 1994

[19] J.O. Smith, *Physical Audio Signal Processing* http://ccrma.stanford.edu/ jos/pasp/, online book, accessed August 2010.

[20] Philip M. Morse and K. Uno Ingard, *Theoretical Acoustics*, Princeton University Press, Princeton, NJ, 1968.

[21] Photo courtesy of Big "D" Broadcast exchange http://www.bigdmc.com/